ation of the two. All kinetic parameters were either directly determined, or derived from experimental measurements (supporting online text).

To model the spreading response, the area of contact between cell and bilayer increased in a series of small steps. The dependence on antigen binding was obtained by stipulating that each successive increment of cell area took place only if the receptor occupancy reached 75%. If this critical occupancy was not attained 1 min after initial attachment (an indication of insufficient antigen or avidity) then the cell "detached" and the simulation was aborted. As soon as receptor occupancy reached 75%, the area of cell attachment was increased by a fixed amount and a new cohort of receptors added. Iterated application of this strategy continued until 2 min after the initial contact with the lipid bilayer, when the area of cell contact began to shrink at a rate based on experimental measurements. Receptor-antigen pairs were collected into the central area (supporting online text).

We found that, given suitable parameters, this simple model was able to reproduce the essential features of the B cell response (Fig. 3F and fig. S4). It had a similar time course of spreading and contraction and it had a comparable capacity to discriminate between different antigen densities and affinities. The quantity of antigen accumulated showed a nonlinear relationship with affinity and density over a wide range (fig. S5A). However, if the spreading mechanism was inactivated in the program, for example by giving the B cell a fixed area of contact, then the amount of antigen accumulated was closely similar for both high- and low-affinity antigens (Fig. 4, A and B)—a result that we also found using the experimental set-up (Fig. 4, C and D, and fig. S2, G and H). These results are consistent with the notion that a quantitative relationship between receptor occupancy and cell spreading may influence the observed cellular response (Fig. 4E). Mechanistic details of this linkage—the role played by the small focal clusters of receptors and how these are coupled to actin accumulation and tyrosine phosphorylation and hence the extension of lamellipodia—will require further collaboration between experiment and theory.

The B cell spreading reported here shares some similarities to the one observed in T cells (*18*–*21*). Both processes are sensitive to inhibitors of signaling and actin polymerization (*20*) and could represent an active process common to lymphocytes in general. In T cells, the process of antigen recognition has been the subject of extensive quantitative studies combined with computer models (*22*–*25*). However, the gathering of antigen by B cells is responsive to a much wider range of antigen affinities than T cells. It will occur in the absence of adhesion molecules without compromising the fundamental features of the antigen-specific responses. This highly reduced experimental system can then be modeled using a simple stochastic algorithm based on the binding interactions between antigen and cell receptors. In this way, we have been able to clarify the basis of the powerful discriminatory ability of B cells.

References and Notes

1. D. M. Russell *et al.*, *Nature* **354**, 308 (1991).
2. S. B. Hartley *et al.*, *Nature* **353**, 765 (1991).
3. J. G. Tew, M. H. Kosco, G. F. Burton, A. K. Szakal, *Immunol. Rev.* **117**, 185 (1990).
4. M. Wykes, A. Pombo, C. Jenkins, G. G. MacPherson, *J. Immunol.* **161**, 1313 (1998).
5. A. M. Haberman, M. J. Shlomchik, *Nat. Rev. Immunol.* **3**, 757 (2003).
6. M. H. Kosco-Vilbois, *Nat. Rev. Immunol.* **3**, 764 (2003).
7. A. Bergtold, D. D. Desai, A. Gavhane, R. Clynes, *Immunity* **23**, 503 (2005).
8. F. D. Batista, D. Iber, M. S. Neuberger, *Nature* **411**, 489 (2001).
9. Y. R. Carrasco, S. J. Fleire, T. Cameron, M. L. Dustin, F. D. Batista, *Immunity* **20**, 589 (2004).
10. C. R. Monks, B. A. Freiberg, H. Kupfer, N. Sciaky, A. Kupfer, *Nature* **395**, 82 (1998).
11. A. Grakoui *et al.*, *Science* **285**, 221 (1999).
12. M. F. Krummel, M. D. Sjaastad, C. Wulfing, M. M. Davis, *Science* **289**, 1349 (2000).
13. C. C. Goodnow *et al.*, *Nature* **334**, 676 (1988).
14. Y. M. Teh, M. S. Neuberger, *J. Exp. Med.* **185**, 1753 (1997).
15. G. T. Williams, C. J. Peaker, K. J. Patel, M. S. Neuberger, *Proc. Natl. Acad. Sci. U.S.A.* **91**, 474 (1994).
16. M. Reth, *Nature* **338**, 383 (1989).
17. S. S. Andrews, D. Bray, *Phys. Biol.* **1**, 137 (2004).
18. S. C. Bunnell *et al.*, *J. Cell Biol.* **158**, 1263 (2002).
19. S. C. Bunnell, V. Kapoor, R. P. Trible, W. Zhang, L. E. Samelson, *Immunity* **14**, 315 (2001).
20. P. A. Negulescu, T. B. Krasieva, A. Khan, H. H. Kerschbaum, M. D. Cahalan, *Immunity* **4**, 421 (1996).
21. M. V. Parsey, G. K. Lewis, *J. Immunol.* **151**, 1881 (1993).
22. N. J. Burroughs, C. Wulfing, *Biophys. J.* **83**, 1784 (2002).
23. K. H. Lee *et al.*, *Science* **302**, 1218 (2003).
24. S. J. Lee, Y. Hori, J. T. Groves, M. L. Dustin, A. K. Chakraborty, *Trends Immunol.* **23**, 500 (2002).
25. Q. J. Li *et al.*, *Nat. Immunol.* **5**, 791 (2004).

26. We thank P. Bates and his group, J. Lewis, K. Lipkow, V. Silva-Vargas, and C. Reis e Sousa for critical reading of this manuscript. We also thank the Electron Microscopy Unit at the London Research Institute. This work was funded by National Institute of General Medical Sciences grant G64713 (D.B.), Cancer Research UK, and the European Molecular Biology Organization Young Investigator Program (F.D.B.).

Supporting Online Material

www.sciencemag.org/cgi/content/full/312/5774/738/DC1
Materials and Methods
SOM Text
Figs. S1 to S5
Table S1
References
Movies S1 to S4

16 December 2005; accepted 13 March 2006
10.1126/science.1123940

Structure of the Multidrug Transporter EmrD from *Escherichia coli*

Yong Yin,* Xiao He,* Paul Szewczyk, That Nguyen, Geoffrey Chang†

EmrD is a multidrug transporter from the Major Facilitator Superfamily that expels amphipathic compounds across the inner membrane of *Escherichia coli*. Here, we report the x-ray structure of EmrD determined to a resolution of 3.5 angstroms. The structure reveals an interior that is composed mostly of hydrophobic residues, which is consistent with its role transporting amphipathic molecules. Two long loops extend into the inner leaflet side of the cell membrane. This region can serve to recognize and bind substrate directly from the lipid bilayer. We propose that multisubstrate specificity, binding, and transport are facilitated by these loop regions and the internal cavity.

The advent of medicinal antibiotics heralded an unprecedented breakthrough in the treatment of infectious disease, but the emergence of drug-resistant bacteria is threatening to undermine this achievement. Multidrug resistance (MDR) develops partially through direct drug efflux by integral membrane transporters. There are two classes of MDR transporters: adenosine 5′-triphosphate (ATP)–binding cassette (ABC) proteins that directly couple drug efflux to ATP hydrolysis and secondary transporters that use energy derived from electrochemical gradients across the cell membrane. The secondary transporters include four families: the Resistance/Nodulation/Division superfamily (RND), the Multiple Antimicrobial Toxin Extrusion family, the Small Multidrug Resistance family, and the Major Facilitator Superfamily (MFS). The MDR transporters from the MFS family (MDR MFS) are among the most prevalent in microbial genomes and diverse in their substrate specificities (*1*).

One MDR MFS transporter, EmrD, is a proton-dependent secondary transporter from *Escherichia coli*. EmrD was first identified as an efflux pump for uncouplers of oxidative phosphorylation (*2*), which can rapidly arrest growth in bacteria by depleting the H^+ gradient (*3*). Some of these uncouplers are structurally unrelated, such as meta–chloro carbonylcyanide

The Scripps Research Institute, Department of Molecular Biology, 10550 North Torrey Pines Road, CB-105, La Jolla, CA 92037, USA.

*These authors contributed equally to this work.
†To whom correspondence should be addressed. E-mail: gchang@scripps.edu

phenylhydrazone (CCCP) and tetrachlorosalicylanilide. It was later discovered that EmrD could also transport detergents such as benzalkonium and sodium dodecylsulfate (*4*). Sequence alignment suggests that EmrD is a close homolog to other MDR MFS transporters (*5*), including NorA from *Staphylococcus aureas* (with 19% identity and 41% similarity), LmrP from *Lactococcus lactis* (22 and 40%), FlorR from *S. enterica* (24 and 45%), Bmr from *Bacillus subtilis* (20 and 40%), and the *E. coli* transporters MdfA (26 and 39%) and Bcr (24 and 44%) (fig. S1). EmrD *E. coli* has 394 amino acids and a molecular weight of ~42.2 kD. Hydropathy analysis indicates that EmrD has 12 transmembrane α helices, and phylogenetic studies have suggested that it is a drug/H^+ antiporter (DHA) from the DHA12 drug efflux subfamily within the MFS (*6*).

The general model for substrate efflux by secondary transporters involves an alternating access mechanism, and most non-MDR MFS transport systems, such as the lactose (LacY) and glycerol-3-phosphate (GlpT) permeases, typically transport a relatively narrow range of structurally related substrates (*7*, *8*). MDR MFS transporters, such as EmrD, differ significantly in that they are able to export a broad spectrum of hydrophobic compounds (*9*). How do they recognize this wide range of structurally distinct substrates and what are the conformational rearrangements within the MFS necessary for hydrophobic drug efflux? To elucidate the molecular basis of MDR MFS transport, we determined the x-ray structure of EmrD to 3.5 Å resolution by anomalous dispersion methods.

Crystals of EmrD were grown in the presence of β-dodecyl-maltoside. X-ray diffraction data was collected from a native crystal and a gold thiomalate derivative (table S1). After density modification and phase extension, the electron density map clearly showed two identical molecules in the asymmetric unit with densities corresponding to side chains (Fig. 1A and fig. S2). The crystal lattice contacts between the two copies of EmrD are small (<250 $Å^2$), and we believe that the packing arrangement of the dimer is nonphysiological. We designate the transmembrane helices in each monomer as H1 to H12 and the connecting loops L1-2 to L11-12.

The overall structural topology of EmrD is reminiscent of LacY and GlpT. Twelve transmembrane helices form a compact structure that spans ~50 Å in the plane of the lipid bilayer and ~45 Å along the membrane normal (Fig. 1, B and C). The transmembrane helices facing away from the interior (H3, H6, H9, and H12) demonstrate an organization similar to LacY and GlpT. The remaining transmembrane helices form the internal cavity, but their relative orientations show substantial deviation from those observed in LacY and GlpT. This structural arrangement may reflect a general architecture of MDR MFS transporters.

Unlike the LacY and GlpT structures, which are both in the configuration facing the cytoplasm, this EmrD structure is not in a V shape and probably represents an intermediate state. The periplasmic loops in EmrD are more imbedded in the cell membrane, and the central loop L6-7 is considerably shorter. A molecular two-fold axis relates the N- and C-terminal halves of EmrD (H1 to H6 and H7 to H12; average root mean square deviation of 0.78 Å for 116 carbon alpha positions) and supports the notion that the MFS arose from recurrent gene duplication of an ancestral six-helix domain (*9*, *10*). The two halves of EmrD, however, are less symmetric than those of LacY or GlpT, and the most notable internal asymmetry is localized to the loop regions on the periplasmic side. For example, L3-4 (residues 92 to 99) is actually a bent helix, whereas L9-10 (residues 285 to 289) is a short loop. Compared with LacY, H6 in

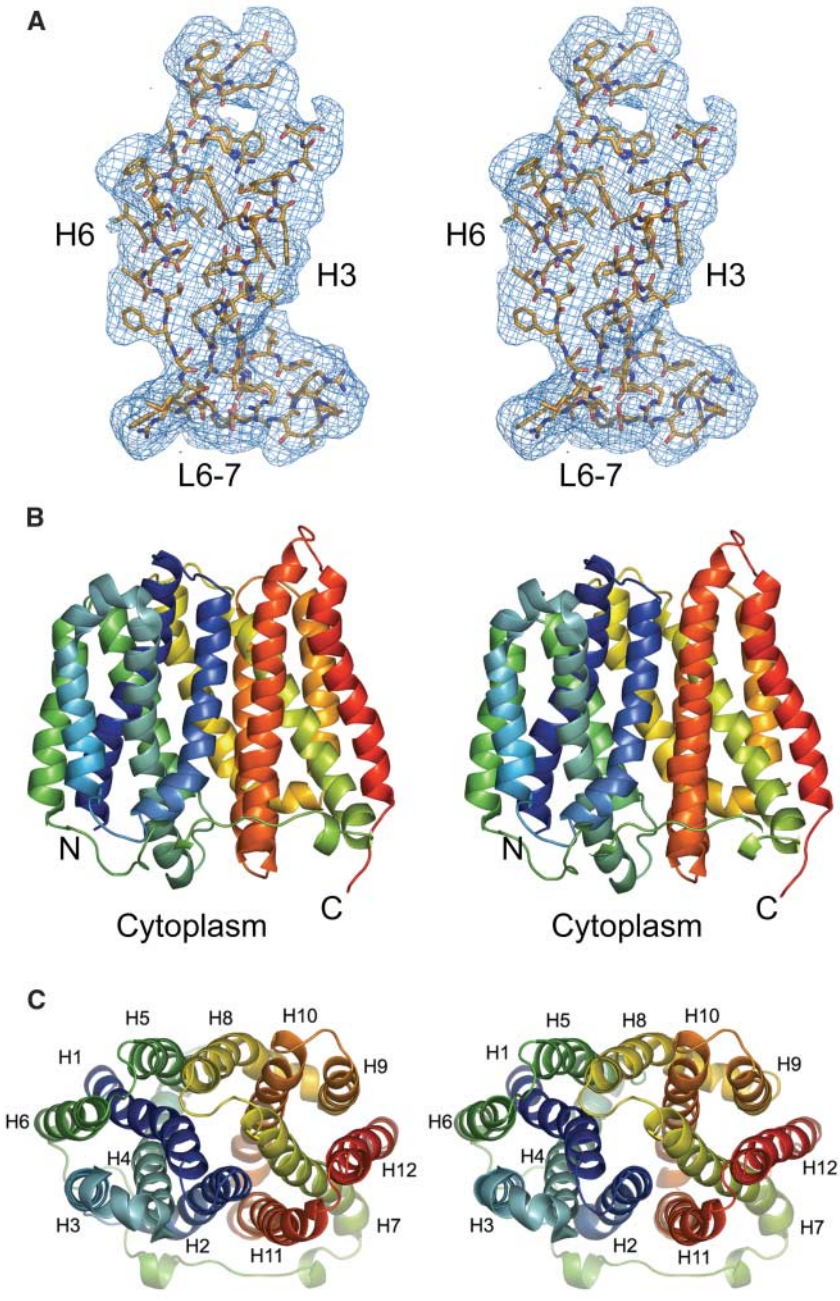

Fig. 1. Stereoimages of crystallography and structure of EmrD. (**A**) A portion of the experimental electron density map is shown for H3, H6, and L6-7. The map is contoured to 1σ. (**B**) Side view of EmrD. The N and C termini are indicated. (**C**) View of EmrD looking toward the cytoplasm showing the molecular two-fold axis relating the N- and C-terminal halves. Transmembrane helices are indicated. The images were created by PyMol (*33*).

EmrD is shorter, whereas H11 is substantially longer.

The most notable difference between the structure of EmrD and the structures of LacY and GlpT is in the internal cavity. Whereas LacY and GlpT have hydrophilic interiors, the internal cavity of EmrD comprises mostly hydrophobic residues, consistent with its function of transporting lipophilic compounds. Several of these residues are bulky and aromatic (Ile^{28}, Ile^{217}, Ile^{253}, Tyr^{52}, Tyr^{56}, Trp^{300}, and Phe^{249}), and some are conserved in other MDR MFS transporters (fig. S1 and Fig. 2, A and B). This type of hydrophobic core has been previously proposed and also observed in the recent x-ray structure of EmrE with substrate (*11*, *12*). These residues likely contribute to a general mechanism of substrate translocation and may play an important role in dictating a level of drug specificity either through steric or aromatic interactions. The internal cavity also has several uncharged polar residues, such as glutamines (Gln^{21}, Gln^{24}, Gln^{46}, and Gln^{60}), and a basic arginine residue (Arg^{118}) that is located closer to the cytoplasmic side. On the periplasmic side lie a threonine (Thr^{25}), an aspartate (Asp^{33}), and a glutamate residue (Glu^{227}) that could easily reorient into the cavity during the transport cycle and may participate in H^+ translocation.

The hydrophobic interior of EmrD provides a generalized pathway and mechanism for transporting a variety of different substrates in drug efflux systems (*11*). EmrD possesses two pairs of stacked aromatic groups (Tyr^{52}/Tyr^{56} and Trp^{300}/Phe^{249}) that could play a key role in multisubstrate binding, given their ability to stack with aromatic drugs (Fig. 2B). In Bmr, two phenylalanines have been implicated in substrate recognition (*13*), whereas the multidrug binding site of the transcriptional repressor QacR uses several aromatic and polar residues (*14*, *15*). The energetic cost of transporting charged amphipathic compounds may be compensated by these types of hydrophobic interactions (*11*).

The structure of EmrD reveals another region that could provide additional substrate specificity. There are two long helical regions (H4, L4-5, H5 and H10, L10-11, and H11) located on the cytoplasmic side that are arranged much closer to the central cavity and extend farther into the cytoplasm than do LacY and GlpT (Fig. 2C). The cytoplasmic end of H4 also has a number of charged residues (Arg^{118}, Arg^{122}, Asp^{123}, Glu^{126}, Arg^{127}, and Arg^{131}), which may play a role both in defining the topology of the transporter and in substrate recognition (*9*). Here, we refer to this region as the selectivity filter. Functional studies of the EmrD homolog MdfA have indicated that several residues in this region are important for substrate recognition. For example, residues in the cytoplasmic halves of H4, H5, and H6 in MdfA are protected by substrate against alkylation by *N*-ethylmaleimide (NEM) (*16*) (Fig. 2C and fig.

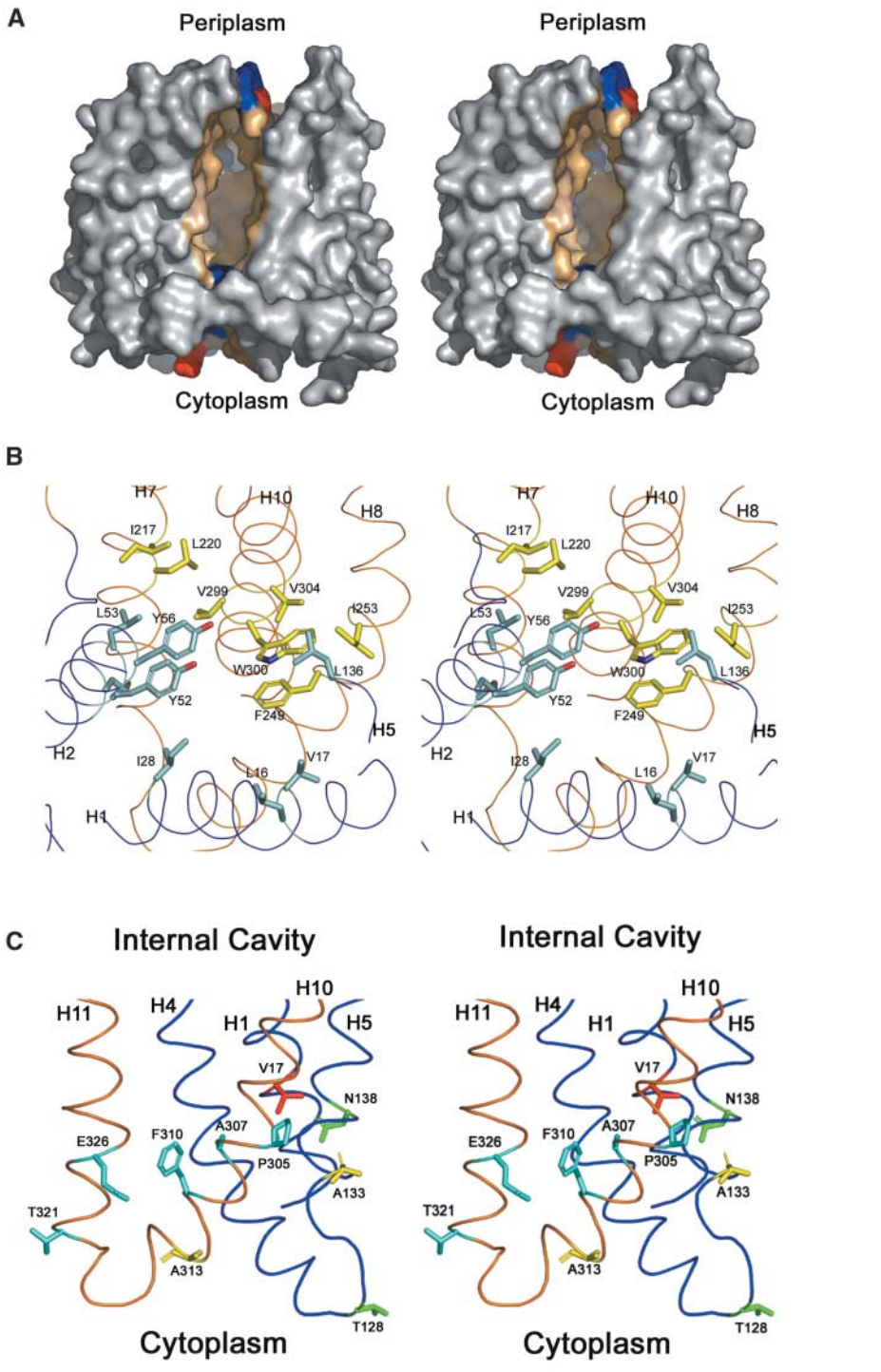

Fig. 2. (**A**) Stereoimage cut-away view of the hydrophobic internal cavity of EmrD. For clarity, residues 43 to 67 were omitted. Hydrophobicity is shown as a gradation from low (light brown) to high (brown). Regions that are positive and negative are shown in blue and red, respectively. (**B**) Stereoimage inside view of the internal cavity of EmrD, characterized by the lining of hydrophobic residues (*34*). The N- and C-terminal halves of EmrD and the corresponding residues are colored blue and orange, respectively. (**C**) Stereoimage close view of the selectivity filter region of EmrD. The positions of residues that are involved in substrate recognition based on protein sequence homology to other MDR MFS transporters are marked in fig. S1. Residues colored in light blue correspond to those in MdfA that, when mutated into cysteines, either reduce or abolish resistance. Residues in yellow correspond to positions in LmrP that are important for substrate recognition. Val^{17}, shown in red, corresponds to Glu^{26} in MdfA and Asp^{23} in FlorR, which are both important for drug recognition. Residues shown in green correspond to cysteine mutations in MdfA that are protected from NEM labeling by substrate. The relative position of the cytoplasm and the internal cavity are indicated.

S1). In addition, certain single-site mutations in the cytoplasmic halves of H10 and H11 as well as L10-11 of MdfA either abolish or substantially reduce MDR (*17*, *18*) (Fig. 2C and fig. S1). Biochemical studies on LmrP, another close homolog of EmrD, also suggest that substantial conformational changes occur in this region. In LmrP, single-site mutations at positions corresponding to 133 and 313 in EmrD show that negative charges in this region are not critical for transport function but are important for drug recognition (Fig. 2C). Further studies on LmrP using fluorescein maleimide labeling upon substrate binding suggest movement of this region from a nonpolar to a polar environment (*18*).

Helix 1 in EmrD might also be important for drug recognition. Studies in MdfA and FlorR have implicated a key residue (Glu^{26} in MdfA and Asp^{23} in FlorR) corresponding to Val^{17} in EmrD that is important for recognizing substrate (*19*, *20*). If this residue is changed to a valine in MdfA, the transporter loses its ability to recognize cationic compounds but still retains wild-type resistance to the neutral antibiotic chloramphenicol (*16*). Interestingly, some other MDR MFS transporters that have small hydrophobic residues at this position are also known to transport neutral hydrophobic compounds. In this EmrD structure, Val^{17} points toward the internal cavity but is also partially accessible from the inner membrane leaflet side (Fig. 2, B and C).

Based on the structure and homology to other MDR MFS transporters, we propose that EmrD intercepts CCCP on the inner membrane leaflet as it crosses toward the cytoplasm (Fig. 3). In the absence of drug efflux, CCCP diffuses across the inner membrane from the periplasmic space in the protonated form, disrupting the pH differential as it moves into the cytoplasm (*3*). The molecule then quickly releases its proton to become a lipophilic soluble anion that rapidly diffuses back to the periplasm (*21*). Binding of CCCP on the inner leaflet side is likely facilitated by the selectivity filter and hydrophobic interactions within the internal cavity of EmrD. Structural rearrangement favoring the outward facing conformation would be coupled to H^+ antiport by a rocker-switch mechanism similar to those previously proposed, but this remains to be proven (*7*, *8*). Based on the structure of EmrD, we speculate that proton translocation and drug transport may occur at different locations, which has also been proposed for MdfA (*11*).

What happens to CCCP when it enters the periplasmic space? There are at least two possibilities. Several MDR MFS systems have an adaptor protein that facilitates the transport of substrate through the periplasmic space; possibly using an apparatus similar to the TolC-adaptor RND efflux systems (*22*–*24*). Perhaps the best known example is the EmrAB efflux system, in which EmrB operates as the MDR MFS transporter and EmrA is an accessory protein (*1*, *25*). In this case, the CCCP would be expelled out of the bacterial cell. However, no such adaptor protein or TolC-like apparatus has been identified that is associated with EmrD or any other 12-TMS MDR MFS transporter. If EmrD acts alone, as do LmrP and Bmr in Gram-positive bacteria, then CCCP would be expelled into the periplasmic space in *E. coli*.

The intracellular loop region of EmrD is reminiscent of the intracellular domain of MsbA, which is a bacterial homolog of MDR ABC transporters (*26*). In MsbA, these helices are thought to recognize head groups of the substrates as well as to transmit structural changes caused by ATP hydrolysis and substrate binding (*27*–*29*). Functional studies on the MDR ABC transporter LmrA suggest a model in which drug recognition by MDR transporters occurs in the inner leaflet of cell membrane bilayer (*30*). The lateral diffusion of hydrophobic substrate has also been proposed for the RND transporter AcrAB/TolC efflux system (*22*, *31*), and access from the inner membrane leaflet is evident in the recent x-ray structures of both EmrE and MsbA with substrate (*12*, *28*). Both of these structures also have hydrophobic pockets. In addition, mutational and biochemical studies on the cytoplasmic side of MdfA and LmrP suggest a model where drugs could diffuse laterally from the inner membrane leaflet (*16*–*18*, *32*). This type of diffusion can be a common theme not only for the MDR MFS but also among all the MDR transporter families.

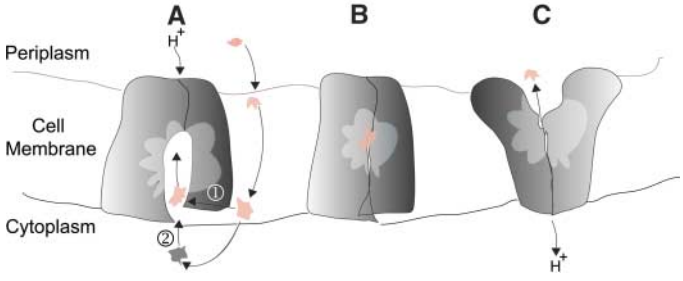

Fig. 3. A potential mechanism for hydrophobic substrate transport by EmrD. (**A**) The drug can enter the internal cavity of the transporter either through the inner membrane leaflet (path 1) or through the cytoplasm (path 2). Substrate recognition and binding may be facilitated through the selectivity filter and the internal cavity containing hydrophobic residues. (**B**) The drug is transported through a rocker-switch alternating-access model coupled with H^+ antiport. (**C**) The drug is transported across the lipid bilayer.

References and Notes

1. M. Putman, H. W. van Veen, W. N. Konings, *Microbiol. Mol. Biol. Rev.* **64**, 672 (2000).
2. V. Naroditskaya, M. J. Schlosser, N. Y. Fang, K. Lewis, *Biochem. Biophys. Res. Commun.* **196**, 803 (1993).
3. T. A. Krulwich, P. G. Quirk, A. A. Guffanti, *Microbiol. Rev.* **54**, 52 (1990).
4. K. Nishino, A. Yamaguchi, *J. Bacteriol.* **183**, 5803 (2001).
5. I. T. Paulsen, M. H. Brown, R. A. Skurray, *Microbiol. Rev.* **60**, 575 (1996).
6. M. H. Saier Jr., C. V. Tran, R. D. Barabote, *Nucleic Acids Res.* **34**, D181 (2006).
7. J. Abramson *et al.*, *Science* **301**, 610 (2003).
8. Y. Huang, M. J. Lemieux, J. Song, M. Auer, D. N. Wang, *Science* **301**, 616 (2003).
9. S. S. Pao, I. T. Paulsen, M. H. Saier, *Microbiol. Rev.* **62**, 1 (1998).
10. M. H. Saier, *Mol. Microbiol.* **48**, 1145 (2003).
11. I. T. Paulsen, K. Lewis, *Microbial Multidrug Efflux* (Horizon Press, Norfolk, 2002).
12. O. Pornillos, Y. J. Chen, A. P. Chen, G. Chang, *Science* **310**, 1950 (2005).
13. K. A. Klyachko, S. Schuldiner, A. A. Neyfakh, *J. Bacteriol.* **179**, 2189 (1997).
14. D. S. Murray, M. A. Schumacher, R. G. Brennan, *J. Biol. Chem.* **279**, 14365 (2004).
15. M. A. Schumacher, M. C. Miller, R. G. Brennan, *EMBO J.* **23**, 2923 (2004).
16. J. Adler, E. Bibi, *J. Biol. Chem.* **279**, 8957 (2004).
17. J. Adler, E. Bibi, *J. Biol. Chem.* **280**, 2721 (2005).
18. P. Mazurkiewicz, W. N. Konings, G. J. Poelarends, *J. Biol. Chem.* **277**, 26081 (2002).
19. R. Edgar, E. Bibi, *EMBO J.* **18**, 822 (1999).
20. M. Braibant, J. Chevalier, E. Chaslus-Dancla, J. M. Pages, A. Cloeckaert, *Antimicrob. Agents Chemother.* **49**, 2965 (2005).
21. J. Kasianowicz, R. Benz, S. McLaughlin, *J. Membr. Biol.* **82**, 179 (1984) (Historical Archive).
22. S. Murakami, R. Nakashima, E. Yamashita, A. Yamaguchi, *Nature* **419**, 587 (2002).
23. J. A. Fralick, *J. Bacteriol.* **178**, 5803 (1996).
24. V. Koronakis, A. Sharff, E. Koronakis, B. Luisi, C. Hughes, *Nature* **405**, 914 (2000).
25. K. Nishino, T. Latifi, E. A. Groisman, *Mol. Microbiol.* **59**, 126 (2006).
26. A. B. Chang, R. Lin, W. K. Studley, C. V. Tran, M. H. Saier, *Mol. Membr. Biol.* **21**, 171 (2004).
27. G. Chang, C. B. Roth, *Science* **293**, 1793 (2001).
28. C. L. Reyes, G. Chang, *Science* **308**, 1028 (2005).
29. B. Woebking *et al.*, *J. Bacteriol.* **187**, 6363 (2005).
30. H. Bolhuis *et al.*, *EMBO J.* **15**, 4239 (1996).
31. E. W. Yu, G. McDermott, H. I. Zgurskaya, H. Nikaido, D. E. Koshland Jr., *Science* **300**, 976 (2003).
32. H. Bolhuis *et al.*, *J. Biol. Chem.* **271**, 24123 (1996).
33. W. L. Delano, PyMol molecular visualization system (http://pymol.sourceforge.net).
34. Single-letter abbreviations for the amino acid residues are as follows: A, Ala; C, Cys; D, Asp; E, Glu; F, Phe; G, Gly; H, His; I, Ile; K, Lys; L, Leu; M, Met; N, Asn; P, Pro; Q, Gln; R, Arg; S, Ser; T, Thr; V, Val; W, Trp; and Y, Tyr.

35. We thank S. Lieu for general lab support and the staff at the Stanford Synchrotron Radiation Laboratory (SSRL) and the Advanced Light Source (beamlines BL821 and BL831) for assistance with data collection and crystal screening. We thank P. Wright, R. Milligan, M. Saier, C. Reyes, S. Aller, and A. Ward for carefully reading and making valuable suggestions to the manuscript. This study was supported by grants from the NIH (GM70480 and GM65798), NASA (NAG8-1834), a NIH Presidential Early Career Award, and the Skaggs Institute for Chemical Biology. Coordinates have been deposited in the Protein Data Bank (PDB code 2GFP).

Supporting Online Material

www.sciencemag.org/cgi/content/full/312/5774/741/DC1
Materials and Methods
Figs. S1 and S2
Table S1
References

31 January 2006; accepted 7 April 2006
10.1126/science.1125629